UC Irvine

UC Irvine Previously Published Works

Title

Intracellular amyloid and the neuronal origin of Alzheimer neuritic plaques

Permalink

https://escholarship.org/uc/item/7n85j4v7

Authors

Pensalfini, Anna
Albay, Ricardo
Rasool, Suhail
et al.

Publication Date

2014-11-01

DOI

10.1016/j.nbd.2014.07.011

Peer reviewed

Intracellular amyloid and the neuronal origin of Alzheimer neuritic plaques

Anna Pensalfini[1,*,a], **Ricardo Albay III**[1], **Suhail Rasool**[1,‡], **Jessica Wu**[1,§], **Asa Hatami**[1,†], **Hiromi Arai**[1], **Lawrence Margol**[1], **Saskia Milton**[1], **Wayne Poon**[2], **Maria Corrada**[2,3], **Claudia Kawas**[2,3,4], and **Charles Glabe**[1,b,5]

[1]Department of Molecular Biology and Biochemistry, University Of California, Irvine, Ca, 92697.

[2]Institute for Memory Impairments and Neurological Disorders, University Of California, Irvine, Ca, 92697.

[3]Department of Neurology, University Of California, Irvine, Ca, 92697.

[4]Department of Neurobiology & Behavior; University Of California, Irvine, Ca, 92697.

[5]Experimental Biochemistry Unit, King Fahd Medical Research Center, King Abdulaziz University, Jeddah, Saudi Arabia.

Abstract

Genetic analysis of familial forms of Alzheimer's disease (AD) causally links the proteolytic processing of the amyloid precursor protein (APP) and AD. However, the specific type of amyloid and mechanisms of amyloid pathogenesis remain unclear. We conducted a detailed analysis of intracellular amyloid with an aggregation specific conformation dependent monoclonal antibody, M78, raised against fibrillar Aß42. M78 immunoreactivity colocalizes with Aß and the carboxyl terminus of APP (APP-CTF) immunoreactivities in perinuclear compartments at intermediate times in 10 mo 3XTg-AD mice, indicating that this represents misfolded and aggregated protein rather than normally folded APP. At 12 mo, M78 immunoreactivity also accumulates in the nucleus. Neuritic plaques at 12 mo display the same spatial organization of centrally colocalized M78, diffuse chromatin and neuronal nuclear NeuN staining surrounded by peripheral M78 and APP-CTF immunoreactivity as observed in neurons, indicating that neuritic plaques arise from degenerating neurons with intracellular amyloid immunoreactivity. The same staining pattern was observed in neuritic plaques in human AD brains, showing elevated intracellular M78 immunoreactivity at intermediate stages of amyloid pathology (Braak A and B) compared to no

[a]**Address correspondence to**: Dr. Anna Pensalfini, apensalfini@NKI.RFMH.ORG. [b] Dr. Charles Glabe, Department of Molecular Biology and Biochemistry, University of California Irvine, Irvine, CA 92697-3900, Phone: 949-824-6081, FAX: 949-824-8551, cglabe@uci.edu.
[*]**Current address**: Center for Dementia Research, Nathan S. Kline Institute, Orangeburg, NY,10962
[‡]Department of Physiology and Neurosciences, New York University School of Medicine, New York, NY, 10016
[§]Department of Pathology and Cell biology, Taub Institute for Alzheimer's Disease Research, Columbia University, New York, NY, 10032
[†]Department of Neurology, David Geffen School of Medicine, University of California, Irvine, CA, 90095

amyloid pathology and late stage amyloid pathology (Braak 0 and C, respectively). These results indicate that intraneuronal protein aggregation and amyloid accumulation is an early event in AD and that neuritic plaques are initiated by the degeneration and death of neurons by a mechanism that may be related to the formation of extracellular traps by neutrophils.

Keywords

Alzheimer; intracellular amyloid; nuclear pathology; neuritic plaques

Introduction

Alzheimer's disease (AD) has traditionally been defined by the presence of extracellular plaques containing aggregated amyloid ß (Aß) and intracellular tangles containing aggregated tau. However, accumulation of aggregated Aß in plaques does not correlate well with disease and many individuals with large amounts of amyloid deposits are not demented (Terry 1996). This suggests that some form of unseen Aß which may accumulate prior to extracellular plaque deposition is more closely associated with pathogenesis. Soon after the discovery of Aß, it was observed that APP and Aß immunoreactivity accumulates in the perinuclear area of a subset of neurons and in the corona of dystrophic neurites surrounding neuritic plaques and it was proposed that this APP represents the penultimate source of Aß accumulating in the core of the neuritic plaques (Selkoe, Podlisny et al. 1988; Grundke-Iqbal, Iqbal et al. 1989; Ikeda, Allsop et al. 1989; Perry, Siedlak et al. 1989; Stern, Otvos L et al. 1989; Arai, Lee et al. 1990; Cummings, Su et al. 1992). However, with the discovery of soluble secreted Aß, this interpretation fell out of favor (Joachim, Games et al. 1991). Many transgenic animal models of AD exhibit intracellular Aß and APP immunoreactivity (reviewed in (Wirths and Bayer 2012)) that precedes cognitive decline and amyloid deposition or that is associated with neuronal loss (Schmitz, Rutten et al. 2004) and synaptic dysfunction (Oddo, Caccamo et al. 2003). Many of the accumulating immunoreactive molecules appear to be APP and/or fragments of APP rather than Aß (Winton, Lee et al. 2011). This could represent the accumulation of normal APP and its metabolites, however the intracellular amyloid in at least two mouse models also reacts with conformation dependent antibodies that recognize pathologically misfolded oligomeric and fibrillar amyloid (Oddo, Caccamo et al. 2006; Ferretti, Partridge et al. 2011; Kulic, McAfoose et al. 2012). Increasing evidence indicates that amyloids are structurally diverse and conformation dependent antibodies can detect these structural differences by the exposure or hiding of their epitopes depending on the particular aggregation state (Kayed, Head et al. 2003; Kayed, Head et al. 2007; Glabe 2008; Kayed, Pensalfini et al. 2009). To investigate whether this conformational diversity is relevant to intracellular amyloid pathogenesis we cloned a panel of conformation dependent antibodies raised against fibrillar Aß 42 and carried out a detailed analysis of intracellular amyloid in 3XTg-AD mouse and human AD brains. We found that M78 immunoreactivity colocalizes with elevated intracellular Aß and APP-CTF immunoreactivity at early times in 3XTg-AD mice and human AD brains. M78 also stains neuronal nuclei at intermediate stages of plaque pathology, whereas at later stages the nuclear staining disappears and M78 immunoreactivity localizes with a subset of amyloid plaques that react only weakly with Aß or APP antibodies. Finally, we found that neuritic

plaques display the same spatial relationships of perinuclear Aß, APP-CTF immunoreactivity and nuclear M78 immunoreactivity that are observed in neurons. Since these plaques also showed a diffuse DNA DAPI and neuronal marker NeuN positive core, we postulate that these plaques arise from the death of single neurons, releasing both chromatin and amyloid in the extracellular space.

Materials and Methods

Antibodies

The antibodies used in this study and the working conditions are listed in Table 1

M78 Antibody production and characterization

Rabbit monoclonal antibody M78 was made under contract with Epitomics (Burlingame, CA) using fibrillar Aß42 as an antigen and immunizing New Zealand white rabbits, as previously described for preparing OC polyclonal serum (Kayed, Head et al. 2007) and, more recently, monoclonal antibodies M64 and M87 (Kayed, Head et al. 2007; Nussbaum, Schilling et al. 2012). Approximately 10,000 pools of hybridomas were screened against Aß42 fibrils, prefibrillar oligomers or monomeric Aß, and 120 pools having an absorbance at least 3-folds above background in ELISA assays were selected for further analysis. Secondary screening consisted of probing blots of a medium density array of 130 different preparations of fibrils, prefibrillar oligomers and monomers of Aβ1-42, Aβ1-40, islet amyloid polypeptide (IAPP), polyQ40, overlapping 15 residue peptide segments of Aß and amyloid-forming random peptides. Hybridoma pools were also probed by immunohistochemistry on human AD and age-matched control brain tissues. Pools giving a unique pattern of immunoreactivity on the array or on immunohistochemistry were selected for cloning and further characterization by immunohistochemistry, western blotting and ELISA. Epitope mapping was performed as previously described (Nussbaum, Schilling et al. 2012). A peptide array (PepSpotsTM) consisting of a series of overlapping 10 mers from the -4 position of the Aß sequence to residue 46 covalently bonded via the carboxyl terminus to a cellulose membrane was prepared by JPT Peptide Technologies GmbH (Berlin, Germany) and used according to the manufacturer's recommendations. 100 ng/ml of primary antibody were added to the membranes, followed by incubation with 1 μg/ml goat anti-rabbit secondary conjugated with alkaline phosphatase and TMB substrate detection (Promega, Madison, WI). The larger the number of contiguous immunopositive spots, the smaller the sequence that the spots have in common. For the antibody blocking experiment, Aß 40 fibrils in HFIP/ddH$_2$O, prepared as described above, were coupled to M-270 Epoxy Dynabeads (Dynal/Invitrogen) at a peptide concentration of 0.2 mg/ml in 0.1M sodium phosphate buffer, pH 7.4, containing 1M ammonium sulphate and incubated overnight at 37 °C under gentle tilting. Aß fibrils were cross-linked to magnetic beads with 0.25% glutaraldehyde in 0.1M sodium phosphate buffer, pH 7.5 for 5 min at room temperature, washed 3 times with PBS and used to affinity purify M78. Briefly, 200 μl of 0.14 mg/ml M78 in PBS were incubated with Aß40-cross-linked magnetic beads for 2 hours at 4 °C. The sample was placed on a magnet and the resultant supernatant was retained as unbound fraction. Fibril bound M78 was eluted with 3M glycine pH 2.0 and immediately neutralized with 1/10 (vol/vol) of 1M Tris pH 8.0. Tissue sections from human AD and 12 mo 3XTg-

AD brains were then processed for immunohistochemistry as described below and probed with unfractionated, fibril bound and fibril unbound M78 at 1.4 μg/ml in TBS-B overnight at room temperature, followed by incubation with anti-rabbit biotinylated secondary antibodies (1:250) and DAB (ABC) detection kit (Vector, Burlingame, CA).

Preparation of Aß40/42, α-synuclein and IAPP fibrils and *in vitro* characterization of M78 immunoreactivity by immunoblot analysis

Lyophilized Aß40 or Aß42 peptides were resuspended in 50% acetonitrile/ddH$_2$O mixture and relyophilized. Fibrils were prepared by dissolving the peptide at 2 mg/ml in 50% hexafluoroisopropanol (HFIP)/ddH$_2$O in a siliconized Eppendorf tube and stirred at 500 rpm with a Teflon coated micro stir bar at room temperature, as previously described (Rasool, Albay et al. 2012). IAPP and alpha-synuclein were dissolved at a concentration of 420 μM in 10 mM NaOH, incubated for 30 minutes at room temperature and diluted to 70 μM in 100mM phosphate buffer without stirring. Sample aliquots were taken at 0-24 hr intervals to test immunoreactivity with M78 antibody by dot blot and western blotting. To test the stability of M78 immunoreactivity to thermal denaturation, Aß40 fibrils were prepared under four different aggregation conditions, as described in (Nussbaum, Schilling et al. 2012) and probed with M78 before or after thermal denaturation at 100 °C for 5 minutes by western blotting. Dot blot and western blotting were performed as previously described (Kayed, Canto et al. 2010).

Human and mouse brain selection

Paraformaldehyde-fixed postmortem human brain tissues were obtained from the UCI ADRC. Subjects enrolled in the ADRC were given the MMSE. As a standard protocol for ADRC autopsy cases, Braak and Braak neurofibrillary tangle and plaque staging was evaluated (Braak and Braak 1991). We examined tissues from the frontal cortex (Brodmann's Areas B4, B9 and B11), hippocampus, and cerebellum based on the progression of ß-amyloid deposition over the course of the disease (Thal, Rub et al. 2002). Table 2 lists clinical and pathological details of the ADRC cases used in this study. Patients were matched for age, gender and post-mortem interval (PMI). There were a total of 28 cases used, 12 were cognitively normal with MMSE scores ranging from 23-30 and without evidence of AD pathology, 1 individual was diagnosed with senile dementia change, having an MMSE score of 22 and insufficient pathology for a diagnosis of AD, and 15 were demented with MMSE scores of 0-19 and AD pathology.

We also examined the frontal cortex (Brodmann's B9) from 21 subjects participating in the *The 90+ Study*, a population-based longitudinal study designed to study aging, dementia and its neuropathological correlates, in individuals 90 years of age and older (Szekely, Green et al. 2008). This group was composed of samples that were selected on the basis of histopathological and psychometric classification as non-demented with insufficient pathology to qualify for a classification of AD (*n* = 6), non-demented with AD pathology (*n*=5), demented with insufficient pathology (*n* = 5) and demented with AD pathology (n=5). The groups with insufficient pathology for a diagnosis of AD included two subjects with Lewy body disease (LBD) and corticobasal degeneration (CBD). Table 3 lists the clinical and pathological characteristics of *The 90+ Study* subjects examined.

3XTg-AD and non-transgenic (non-Tg) mice were provided by the UCI-Alzheimer's disease research center from animals maintained in accordance with institutional guidelines (Oddo, Caccamo et al. 2003). In particular, brains from 3XTg-AD mice aged at 3, 10, 12 and 14 months and age-matched non-Tg counterparts (n = 4 mice per age group) were used in this study. Brain sections from 6-month-old 5XFAD mice were also examined (kindly provided by Dr. Zhiqun Tan, Department of Neurology, University of California Irvine School of Medicine).

Immunohistochemistry

Paraformaldehyde-fixed brain tissues from AD patients and age-matched controls, as well as from 3XTg-AD and non-Tg mice, were sectioned with a vibratome (40 μm). Free floating sections were collected in PBS, 0.02% NaN_3, pH 7.4 and stored at 4 °C prior to staining. Endogenous peroxidase was blocked by treating with 3% H_2O_2 and 10% methanol (vol/vol) in Tris-buffered saline (TBS), (20 mM Tris and 137 mM NaCl, pH 7.5) for 30 min at room temperature. Sections were permeabilized in 0.1% Triton X-100 (TX) for 15 min, blocked by 30 min incubation in TBS containing 2% BSA, 0.1% TX (TBS-B) and probed with primary antibodies in TBS-B overnight at room temperature (for antibody specifications, antigen retrieval methods and working dilutions see Table 1). After rinsing 3 times with TBS, 0.1% TX, sections were blocked in TBS-B for 15 minutes and incubated with anti-mouse or anti-rabbit biotinylated secondary antibodies (1:250) in the presence of 1.5% normal horse or goat serum, respectively, followed by detection with an ABC peroxidase kit, and visualization with a 3,3'-diaminobenzidine (DAB) substrate kit (Vector, Burlingame, CA).

Immunofluorescence

To address whether M78 colocalizes with any Aß/APP antibodies and identify which cell types are associated with M78 immunoreactivity, human AD and 3XTg-AD mouse brain sections were processed for double immunofluorescence. After blocking with TBS-B, primary antibodies from different species (see Table 1) were simultaneously added to the sections and incubated overnight at room temperature. This was followed by 3 washes in TBS, 0.1% TX, blocking in TBS-B for 15 min and incubation with anti-mouse and anti-rabbit secondary antibodies coupled to Alexa Fluor 488 or Alexa Fluor 660 (Invitrogen, CA), respectively, overnight at room temperature. For double labeling M78 and other rabbit antibodies (glial fibrilliary acidic protein (GFAP) and anti-APP-CTF), anti-GFAP or anti-APP-CTF was incubated with the sections first which were then processed as for single immunofluorescence. After the addition of an Alexa Fluor 488 dye-conjugated goat anti-rabbit secondary antibody (Invitrogen, CA), sections were washed 3 times with TBS and incubated for 3 hours with 2% paraformaldehyde at 37 °C. Sections were then washed 3 times with TBS, permeabilized with TBS, 0.1% TX, and blocked in TBS-B containing 20 μg/ml of normal rabbit serum for 1 hour at room temperature, followed by incubation with M78-Alexa Fluor 647 (monoclonal antibody labeling kit, Invitrogen, CA) overnight at room temperature. Cell nuclei were counterstained using 1 μM DAPI or Hoechst 33258 in PBS for 20 min at room temperature. Images were captured using a ZEISS LSM 780 confocal microscope equipped with an argon-ion laser source for fluorescence measurements, using 405, 488 and 633 nm excitation wavelengths for DAPI, Alexa 488 and Alexa 660,

respectively. A series of optical sections (1024×1024 pixels) 15 μm in thickness was taken through the tissue depth at intervals of 1.5 μm using Plan-Apochromat $40 \times / 1.3$ or $63X / 1.40$ oil immersion objectives. Images were then projected as a single composite image by superimposition using the Zeiss LSM image analysis software.

M78 correlation with AD pathology and statistical analysis

M78 positive nuclei in the hippocampal region (CA1) of 3, 10, 12 and 14 month 3XTg-AD and wild type mice or in the frontal cortex of human brains were manually counted from confocal microscopy images. 6 to 8 (317.3 μm $\times$ 317.3 μm) fields were analyzed from at least 3 independent experiments and the average counts/mm^2 were plotted against different ages in mice or against the Braak and Braak Plaque Stage in humans, considering plaque stage 0 = no AD pathology; plaque stage A-B = intermediate pathology / intermediate area of plaque deposition; plaque stage C = late AD pathology / high plaque area. For the analysis that combined subjects enrolled in the ADRC and subjects participating in *The 90+ Study*, the area fraction occupied by OC plaques was obtained from immunohistochemical staining of the frontal cortex of 47 subjects and 6 (500 μm $\times$ 500 μm) fields per subject were analyzed. Three major categories were defined based on the OC area fraction and represented by low (< 1%, average OC counts per mm^2 ± SEM = 144.3 ± 24.0, n = 15), intermediate (1-10%, average OC counts per mm^2 ± SEM = 673.15 ± 84.3, *n* = 12) and high (>10%, average OC counts per mm^2 ± SEM = 900.0 ± 55.8, *n* = 20) OC immunoreactivity. Based on this classification, the average counts per mm^2 of M78 positive nuclei in the frontal cortex of each subject were plotted against the OC plaque area fraction. All measurements were performed using the free Java image processing program (ImageJ). Statistical analysis was performed using OriginPro 8 (OriginLab Corp., Northampton, MA). Statistical differences between groups were determined by One-way ANOVA followed by Bonferroni's post-hoc comparisons tests.

Preparation of human brain nuclear lysates and western blot analysis

Frozen tissues from the B11 area were weighted, diced and homogenized in ice-cold PBS, 0.02% NaN3, pH 7.4 with protease inhibitor cocktail as previously described (Tomic, Pensalfini et al. 2009). Brain homogenates were spun at $250 \times g$ for 5 min at 4 °C and the pellet was resuspended in hypotonic buffer (20 mM Tris-HCl, pH 7.4, 10 mM NaCl, 3 mM MgCl2) with protease inhibitor cocktail (PIC), 1 mM phenylmethanesulfonyl fluoride (PMSF) and 1 mM dithiothreitol (DTT), vortexed briefly and set on ice for 15 minutes. Triton X-100 was then added to the same tube to a final concentration of 0.5% (vol/vol), followed by 10 sec vortexing at the highest setting. Nuclei were separated from the cytoplasm by centrifugation at $750 \times g$ for 10 minutes at 4°C and resuspend in 3 volumes (relative to nuclear pellet) of nuclear extraction buffer (100 mM Tris-HCl, pH 7.4, 100 mM NaCl, 1% Triton, 1 mM EDTA, 1mM EGTA,10% glycerol, 0.1% SDS, 0.5 % deoxycholate, 2mM Na_3VO_4, 1 mM NaF, 20 mM $Na_4P_2O_7$) with PIC, 1 mM PMSF and 1 mM DTT, followed by incubation for 30 minutes on ice and sonication 2×5" on ice. The total protein concentration of the nuclear lysate was determined by the BCA Protein Assay (Thermo Scientific, Rockford, IL).

To test the stability of M78 nuclear immunoreactivity to chemical denaturation, nuclear lysates were treated with 50% HFIP or 70% formic acid for 15 minutes and 5 minutes at room temperature, respectively. Samples were subject to a gentle stream of N_2 to evaporate the solvents, resuspended in denaturing Laemmli Sample buffer and probed with M78 and 6E10 by western blotting, before or after thermal denaturation at 100 °C for 5 minutes.

Results

In vitro characterization of M78 immunoreactivity

We cloned a panel of 23 monoclonal antibodies from rabbits that were immunized against Aß 42 fibrils and producing fibril specific OC serum (Kayed, Head et al. 2007). These antibodies demonstrate distinct conformational and linear sequence dependent epitope specificities when screened against a medium density array of 132 different types of Aß, IAPP, α-synuclein and polyQ aggregates and linear Aß segments as described in Supplementary Materials (Nussbaum, Schilling et al. 2012; McLean, Cooke et al. 2013). Several of these aggregation specific monoclonals recognize intracellular amyloid that is stained by 6E10 and antibodies against APP. One of the monoclonals that recognizes intracellular amyloid is M78, which recognizes a discontinuous epitope in the Aß sequence that corresponds to a generic amyloid fibril specific epitope (Fig. 1a). The epitope recognized by M78 is common to amyloid fibrils of unrelated sequence, such as islet amyloid polypeptide (IAPP) and α-synuclein fibrils. However, M78 does not recognize the monomeric forms of any of these amyloidogenic proteins and peptides at time zero (Fig. 1b and Fig. S4). On western blots, M78 stains Aß, α-synuclein and IAPP aggregates with sizes ranging from dimer to material that is retained at the top of the gel (Fig. 1c). The conformational epitope recognized by M78 is stable and resists thermal denaturation at 100 °C (Fig. 1d).

Intraneuronal and nuclear amyloid fibril immunoreactivity accumulates in 10-12 mo 3XTg-AD mice

In 3XTg-AD mice at 3 mo, elevated 6E10 immunoreactivity is observed in a subset of neurons in CA1, but no M78 immunoreactivity is detected indicating that native APP accumulation precedes misfolding and aggregation (Fig. 2a). At 10 mo, the intraneuronal perinuclear Aß immunoreactivity colocalizes with fibril specific M78 immunoreactivity in neurons (Fig. 2b). The fact that the intraneuronal 6E10 immunoreactivity colocalizes with M78 indicates that the 6E10 immunoreactive material is misfolded and has the same aggregated conformation as amyloid fibrils, regardless of whether it is Aß or the Aß sequence contained within APP fragments. At 12 mo, the M78 immunoreactivity is primarily nuclear, but remains surrounded by perinuclear M78 and 6E10 immunoreactivity (Fig. 2c). Nuclear M78 immunoreactivity is no longer detectable at 14 mo and primarily plaque staining is observed (Fig. 2d). Most of the M78 positive plaques in 14 mo 3XTg-AD stain only weakly with 6E10, even after antigen retrieval methods optimized for plaque staining by 6E10. No M78 immunoreactivity is observed in wild type mice at 14 mo (Fig. 2e). Changes in M78 nuclear immunoreactivity as a function of age in the CA1 region of 3XTg-AD and wild type mice were quantified and results are shown in Fig. S1. A significant increase in the counts per mm^2 of M78 positive nuclei is observed in 12 mo

3XTg-AD, representing about 75% of the total nuclei counted (75.9 ± 7.7 %). Only a small number of the total nuclei are weakly positive for M78 at 3 mo (3.9 ± 1.4 %), 10 mo (14.2 ± 2.2 %), and 14 mo (6.6 ± 5.3 %) 3XTg-AD and completely negative in wild type controls (Fig. S1). Similar nuclear M78 immunoreactivity was observed in 6 mo 5X-FAD mice (Fig. S2), indicating that intranuclear M78 staining is not unique to 3XTg-AD mice.

Nuclear M78 and NeuN immunoreactivities are localized in the center of neuritic plaques surrounded by M78 and APP-CTF positive dystrophic neurites

At 12 mo, large numbers of neuritic plaques are found in the subiculum of 3XTg-AD mice (representing approximately 62.41 ± 21.47 % of the total M78 plaques), as compared to 10 mo (20.94 ± 10.44 %) and 14 mo-old mice (42.29 ± 17.60 %). The centers of many of these plaques contain diffuse areas of DAPI chromatin fluorescence that colocalize with M78 immunoreactivity. Approximately 48.4 ± 1.5 % of the M78 positive neuritic plaques have diffuse DAPI positive cores (arrows, Fig. 2f). The DAPI fluorescence in the core is broader and more diffuse than that of adjacent neuronal nuclei, suggesting that the nuclei may be lysed and releasing chromatin. The diffuse chromatin in the center is also stained by Hoechst 33258 (Fig. S3). Dystrophic neurites that are immunopositive for both M78 and APP-CTF are found surrounding the DAPI and M78 positive core. The idea that the chromatin at the center of the neuritic plaque is derived from neuronal nuclei is supported by the observation that most of the cores of neuritic plaques are positive for the neuronal nuclear marker, NeuN (Fig. 2g). These results indicate that neuritic plaques have the same spatial organization of DAPI, M78 and APPCTF staining as observed in the M78 positive neurons at earlier time points, suggesting that neuritic plaques arise from the degeneration of neurons with M78 positive nuclei. We further addressed the specificity of M78 immunoreactivity by blocking the staining with fibrillar Aß40 (Fig. S4). Adsorption of the M78 antibody with fibrillar Aß40 coupled to Dynabeads completely removed both nuclear and plaque staining, whereas it was still observed by using the antibody eluted from the fibril coated beads. These results indicate that the nuclear M78 antigen shares the same epitope as fibrillar Aß.

M78 stains nuclei at intermediate stages of amyloid plaque deposition in human AD brains

M78 also stains nuclei in a subset of human brains that have neurons with intracellular amyloid that stains with 6E10 (Fig. 3a,b). Neurons, astrocytes and oligodendrocytes in these sections also have nuclei that stain with M78 (Fig. 3c-e). Unlike neurons, astrocytes and oligodendrocytes with M78 nuclear staining do not exhibit perinuclear 6E10 or M78 immunoreactivity. Double label confocal immunofluorescence microscopy of the same sample shown in Figure 3a and 3b indicates that the neurons with elevated 6E10 immunoreactivity also contain M78 positive nuclei (Fig. 3f). It also clearly shows that the perinuclear 6E10 immunoreactivity in the soma is also colocalized with M78 immunoreactivity and some 6E10 immunoreactivity is also observed in the nuclei of these neurons. The specificity of the M78 nuclear staining in this sample was confirmed by blocking M78 immunoreactivity with fibrillar Aß40 (Fig. S4).

In order to determine the relationship between M78 positive nuclei and neurodegenerative pathology in human brain, we examined 28 brains obtained from the UC Irvine Alzheimer's Disease Research Center (ADRC) brain bank. This group consists of 12 cognitively normal

individuals with mini mental state examination (MMSE) scores ranging from 23-30, 15 AD individuals with MMSE scores of 0-19 and one individual diagnosed with senile dementia changes with an MMSE score of 22 (Table 2). The number of M78 positive nuclei was determined in the frontal cortex (B11) of each brain (Fig. 3g). Analysis of the distribution of M78 positive nuclei indicates that they are preferentially associated with Braak and Braak plaque stages A and B, compared to stage 0 ($P<0.05$) or stage C ($P<0.01$), suggesting that they are associated with early stages of AD. No significant correlation was observed between M78 positive nuclei and tangle stage or MMSE. We also examined 21 brains from subjects that were older than 90 years (Table 3). This group contained samples that were selected on the basis of histopathological and psychometric classification as non-demented with insufficient pathology to qualify for a classification of AD (NDIP), non-demented with AD pathology (NDAP), demented with insufficient pathology (DIP) and demented with AD pathology (DAP). Although no statistically significant correlation between M78 positive nuclei and plaque stage, tangle stage or MMSE was observed in this group, combined analysis of the samples from the ADRC and the 90+ cohorts on the basis of the total amyloid plaque area stained by OC showed that M78 positive nuclei are significantly elevated in samples that contain an intermediate amount of plaque area (1-10%) compared to no plaques (<1%) or high plaque area (>10%) ($P<0.05$) (Fig. 3h). This suggests that M78 positive nuclei are abundant at early phases of plaque deposition and decline with increasing plaque area. Additionally, samples grouped on the basis of plaque staining showed a significant decrease ($p < 0.05$) in the MMSE at intermediate amount of plaque area (15.1 ± 3.4) compared to the no plaque group (25 ± 1.9).

We also examined neuritic plaques in the frontal cortex of human AD brains. We found that as in 3XTg-AD brain neuritic plaques stain with M78 and antibodies directed against the carboxyl-terminus of APP (Fig. 3i). As shown by three color immunofluorescence staining, these plaques contain diffuse DAPI DNA fluorescence and M78 immunoreactivity in the center and are surrounded by APP-CTF positive neurites, similar to what we observed in 3XTg-AD. These results further support the idea that neuritic plaques may arise from degenerating neurons that contain intracellular amyloid in human brain.

Localization of nuclear M78 immunoreactivity varies in human brain

To determine the extent of nuclear M78 immunoreactivity in human brain, we also examined several regions of the frontal cortex (Broadman's B4, B9, and B11), the hippocampus and the cerebellum of three brains that displayed cortical immunoreactivity (Fig. S5). M78 positive nuclei were observed in all cortical regions of all three brains, in the cerebellum of two brains and the hippocampus of one brain. M78 only stained plaques in the hippocampus of one brain and exhibited weak staining of neuronal somas in another sample. In all cases, the M78 positive nuclei are colocalized with 6E10 staining of neuronal somas. These results indicate that the nuclear M78 immunoreactivity is widespread in some human brain samples and can vary by region in different samples.

M78 positive nuclei material is aggregated, insoluble and resistant to thermal and chemical denaturation

We investigated the nature of the M78 immunoreactive material in M78 positive nuclei purified from cognitively normal brain and brain with a diagnosis of AD (Fig. S6). Western blot analysis of M78 positive nuclei shows that M78 stains high molecular weight, insoluble material in both normal and AD brain that stays on top of the gel, and that this immunoreactivity increases after chemical treatment with 50% HFIP or 70% formic acid or thermal denaturation at 100 °C for 5 min. (Fig. S6, upper blot). In contrast, 6E10 stains full length APP in both normal and AD untreated samples and insoluble aggregates only in the AD brain. After chemical and thermal denaturation, 6E10 no longer stains the soluble full length APP, but it still recognizes high molecular weight insoluble aggregates in the AD brain (Fig. S6, middle blot). M78 does not react with soluble APP-CTF bands stained by an antibody directed against the carboxyl terminus of APP (anti-APP-CFT, Fig 6, lower blot), which also stains insoluble aggregates at the top of the gel. These results indicate M78 does not recognize soluble APP or soluble APP-CTFs and that nuclear M78 positive material is aggregated, stable to chemical and thermal denaturation and resistant to solubilization.

Discussion

Our findings support a novel mechanism of early AD pathogenesis whereby Aß, APP or APP-CTFs begin to accumulate and aggregate intracellularly into a conformation that is recognized by M78 in a perinuclear compartment. This new pathway of neuritic plaque genesis from neurons is summarized in Fig.4. M78 accumulation occurs in a perinuclear compartment prior to the development of significant amounts of plaques and cognitive deficits in humans and at intermediate times (10 months) in 3XTg-AD mice. At intermediate stages of human plaque pathology and in 12 mo 3XTg-AD mice, M78 immunoreactivity is also nuclear, whereas in late stages of AD and 14 mo 3XTg-AD mice, the nuclear immunoreactivity is no longer apparent and M78 stains extracellular plaques. These observations are consistent with previous findings showing a decrease in intraneuronal Aß immunoreactivity with increasing cognitive dysfunction and increasing amyloid plaque deposition (Gouras, Tsai et al. 2000). The large number of neuritic plaques found in the subiculum of 12 mo 3XTg-AD mice displaying the same spatial relationships of central nuclear M78 and DAPI DNA staining surrounded by perinuclear M78, Aß and APP-CTF immunoreactivity observed in neurons suggests that neuritic plaques arise from degenerating neurons containing M78 positive nuclei. The core of these neuritic plaques displays diffuse DAPI DNA fluorescence and NeuN immunoreactivity, providing further evidence of its neuronal nuclear origin.

Intracellular accumulation of Aß and lysis of Aß-loaded pyramidal neurons has previously been proposed as a major source of neuronal loss and amyloid plaque formation in AD (D'Andrea, Nagele et al. 2001). Similarly, recent findings propose a direct link between intracellular Aß/APP-CTF accumulation and appearance of dystrophic neurites in early AD through the amyloid-induced aggregation of the endoplasmic reticulum protein reticulon3 (RTN3), which has been shown to be a negative modulator of ß-site APP cleaving enzyme 1 (BACE1) activity and to accumulate in dystrophic neurites of AD brains before cognitive

dysfunction (Hu, Shi et al. 2007). The remnant of the degenerative neuron would serve as the nidus of the senile plaque and the non-Aß remnants could be removed by the action microglia and the plaque could grow by the peripheral deposition of more Aß from soluble, secreted Aß . The extracellular release of neuronal chromatin we observe is similar to the formation of "extracellular traps" (ETs) during the innate immune response by neutrophils in sepsis, indicating that the mechanism of neuronal cell death may be related to "ETosis" of leukocytes (Wartha and Henriques-Normark 2008). It is conceivable that the extracellular traps may serve the same function in AD by limiting the dissemination of a transmissible amyloid seeding agent to neighboring cells.

The pathological consequences of intracellular amyloid and nuclear accumulation of M78 immunoreactivity are not yet entirely clear, but the data suggest that they precede cognitive dysfunction by many years in humans. Many of the samples exhibiting the highest amounts of M78 positive nuclei come from cognitively normal individuals indicating that these changes are temporally dissociated from cognitive dysfunction, consistent with the growing consensus that AD pathology begins long before cognitive deficits are manifest. In the 3XTg-AD mouse, where the M78 accumulation is more rapid and synchronous, the nuclear M78 immunoreactivity correlates more closely with behavioral impairment, but it still precedes significant Aß plaque deposition (Oddo, Caccamo et al. 2003). The dissociation between intracellular amyloid accumulation and cognitive dysfunction indicates that neuronal function may be maintained even in the presence of intracellular amyloid. If individual neurons die as a result of the initiation of a neuritic plaque, then this would imply that relatively few neurons would be expected to die by this mechanism until plaque deposition is florid and a large volume of the brain is occupied by senile plaques.

The hypothesis that the perinuclear accumulation of M78 immunoreactive aggregated APP-CTF is a key event in AD pathogenesis is consistent with the effects of genetic mutations in familial Alzheimer's disease genes that are the foundation of the amyloid hypothesis. We have proposed an "alternative" amyloid hypothesis that takes into account the intracellular aggregation of amyloid prior to neuritic plaque formation and new observations on the effect of γ-secretase inhibitors in human clinical trials (Fig. 5). Mutations in APP that favor BACE1 cleavage produce more APP ß-CTF, which would be expected to favor its aggregation, while mutations at the ß cleavage site that are protective against AD also decrease the steady state levels of ß-CTF (Jonsson, Atwal et al. 2012). Both types of mutations have the same effect on Aß secretion as on ß-CTF levels. Previous interpretations of the effects of presenilins (PS) 1 and 2 were widely believed to favor the secretion of the longer and more aggregation prone Aß42 isoform over shorter Aß species, but more recent evidence indicates that the FAD PS mutations also represent loss of enzymatic processivity of the mutant allele and result in the production of longer Aß species (Citron, Westaway et al. 1997; Bentahir, Nyabi et al. 2006; Robakis 2011; Cacquevel, Aeschbach et al. 2012). These "long" Aß species may be retained intracellularly rather than secreted. The PS mutations also increase in the steady state levels of ß-CTF, which would favor its aggregation (Cacquevel, Aeschbach et al. 2012). Although the effects of FAD mutations support both the elevated secretion of Aß42 and an increase in retained long Aß and ß-CTF levels as key events in AD, the results from human clinical trials of γ-secretase inhibitors suggest that retained long Aß and ß-CTF may be more important than secreted Aß. While γ-

secretase inhibitors lowered the secretion of Aß in humans, the treated group actually exhibited accelerated cognitive decline (Doody, Raman et al. 2013). This indicates that inhibiting secretion of Aß accelerates pathogenesis. γ-secretase inhibitors also increase the levels of long Aß and ß-CTF, suggesting that the partial inhibition of γ-secretase mimics the primary effect of PS FAD mutations.

It is also worth contemplating why the nuclear amyloid immunoreactivity we observed with M78 has not been previously reported despite the numerous studies of Aß and plaque immunohistochemistry. Clearly, the unique properties of M78 have something to do with it. One potential explanation is that the nuclear immunoreactivity is due to the accumulation of aggregated Aß containing fragments of APP, but this material is aggregated in such a way as to hide the epitopes for typical Aß antibodies, such as 4G8 and 6E10. We have previously reported that 6E10 and 4G8 epitopes are hidden in some types of Aß aggregates in vitro (Necula, Kayed et al. 2007). Consistent with this possibility, we find that pretreatment of the sections with 99% formic acid instead of the commonly used 70% formic acid reveals some intranuclear 6E10 (Fig. 3f). Previous studies have shown that pretreatment of sections with 99% formic acid increases total Aß immunoreactivity by nearly 2-fold (Cummings, Mason et al. 2002). The reliance on two antibodies and a standard 70% formic acid antigen retrieval method may account for much of the non-observation of intranuclear staining. Although M78 recognizes a discontinuous epitope within the Aß sequence, it is clear that the epitope recognized by M78 does not depend on the Aß sequence because it also recognizes amyloid fibrils formed from unrelated protein sequences, such as α-synuclein and IAPP (Fig. 1). Because of the fact that M78 recognizes amyloid fibrils from several amyloidogenic sequences, other possible explanation for the lack of nuclear Aß staining could be that some other type of amyloid is accumulating. However, the fact that we only observe M78 nuclear immunoreactivity in transgenic mice and not wild type argues that the amyloid immunoreactivity is due to transgene expression. If the nuclear amyloid is not directly due to transgene expression, then it must be downstream from transgene expression. The resolution of this issue must await the precise characterization of what is actually accumulating in the nucleus, but this is a daunting task because of the extreme insolubility of the material that is accumulating.

Supplementary Material

Refer to Web version on PubMed Central for supplementary material.

Acknowledgments

References

Arai H, Lee VM, et al. Defined neurofilament, tau, and beta-amyloid precursor protein epitopes distinguish Alzheimer from non-Alzheimer senile plaques. Proc Natl Acad Sci U S A. 1990; 87(6): 2249–2253. [PubMed: 1690426]

Bentahir M, Nyabi O, et al. Presenilin clinical mutations can affect gamma-secretase activity by different mechanisms. J Neurochem. 2006; 96(3):732–742. [PubMed: 16405513]

Braak H, Braak E. Demonstration of amyloid deposits and neurofibrillary changes in whole brain sections. Brain Pathol. 1991; 1(3):213–216. [PubMed: 1669710]

Cacquevel M, Aeschbach L, et al. Alzheimer's disease-linked mutations in presenilin-1 result in a drastic loss of activity in purified gamma-secretase complexes. PLoS One. 2012; 7(4):e35133. [PubMed: 22529981]

Citron M, Westaway D, et al. Mutant presenilins of Alzheimer's disease increase production of 42-residue amyloid beta-protein in both transfected cells and transgenic mice. Nat Med. 1997; 3(1):67–72. [PubMed: 8986743]

Cummings BJ, Mason AJ, et al. Optimization of techniques for the maximal detection and quantification of Alzheimer's-related neuropathology with digital imaging. Neurobiol Aging. 2002; 23(2):161–170. [PubMed: 11804699]

Cummings BJ, Su JH, et al. Aggregation of the amyloid precursor protein within degenerating neurons and dystrophic neurites in Alzheimer's disease. Neuroscience. 1992; 48:763–777. [PubMed: 1378573]

D'Andrea MR, Nagele RG, et al. Evidence that neurones accumulating amyloid can undergo lysis to form amyloid plaques in Alzheimer's disease. Histopathology. 2001; 38(2):120–134. [PubMed: 11207825]

Doody RS, Raman R, et al. A phase 3 trial of semagacestat for treatment of Alzheimer's disease. N Engl J Med. 2013; 369(4):341–350. [PubMed: 23883379]

Ferretti MT, Partridge V, et al. Transgenic mice as a model of pre-clinical Alzheimer's disease. Curr Alzheimer Res. 2011; 8(1):4–23. [PubMed: 21143159]

Glabe CG. Structural classification of toxic amyloid oligomers. J Biol Chem. 2008; 283(44):29639–29643. [PubMed: 18723507]

Gouras GK, Tsai J, et al. Intraneuronal Abeta42 accumulation in human brain. Am J Pathol. 2000; 156(1):15–20. [PubMed: 10623648]

Grundke-Iqbal I, Iqbal K, et al. Amyloid protein and neurofibrillary tangles coexist in the same neuron in Alzheimer disease. Proc. Natl. Acad. Sci. U. S. A. 1989; 86:2853–2857. [PubMed: 2649895]

Hu X, Shi Q, et al. Transgenic mice overexpressing reticulon 3 develop neuritic abnormalities. EMBO J. 2007; 26(11):2755–2767. [PubMed: 17476306]

Ikeda S, Allsop D, et al. A study of the morphology and distribution of amyloid beta protein immunoreactive plaque and related lesions in the brains of Alzheimer's disease and adult Down's syndrome. Prog. Clin. Biol. Res. 1989; 317:313–323. [PubMed: 2532370]

Joachim C, Games D, et al. Antibodies to non-beta regions of the beta-amyloid precursor protein detect a subset of senile plaques. Am. J. Pathol. 1991; 138:373–384. [PubMed: 1704190]

Jonsson T, Atwal JK, et al. A mutation in APP protects against Alzheimer's disease and age-related cognitive decline. Nature. 2012; 488(7409):96–99. [PubMed: 22801501]

Kayed R, Canto I, et al. Conformation dependent monoclonal antibodies distinguish different replicating strains or conformers of prefibrillar Abeta oligomers. Mol Neurodegener. 2010; 5:57. [PubMed: 21144050]

Kayed R, Head E, et al. Fibril specific, conformation dependent antibodies recognize a generic epitope common to amyloid fibrils and fibrillar oligomers that is absent in prefibrillar oligomers. Mol Neurodegener. 2007; 2(18):18. [PubMed: 17897471]

Kayed R, Head E, et al. Common structure of soluble amyloid oligomers implies common mechanism of pathogenesis. Science. 2003; 300(5618):486–489. [PubMed: 12702875]

Kayed R, Pensalfini A, et al. Annular protofibrils are a structurally and functionally distinct type of amyloid oligomer. J Biol Chem. 2009; 284(7):4230–4237. [PubMed: 19098006]

Kulic L, McAfoose J, et al. Early accumulation of intracellular fibrillar oligomers and late congophilic amyloid angiopathy in mice expressing the Osaka intra-Abeta APP mutation. Transl Psychiatry. 2012; 2:e183. [PubMed: 23149447]

McLean D, Cooke MJ, et al. Positron Emission Tomography Imaging of Fibrillar Parenchymal and Vascular Amyloid-beta in TgCRND8 Mice. ACS Chem Neurosci. 2013; 4(4):613–623. [PubMed: 23509918]

Necula M, Kayed R, et al. Small molecule inhibitors of aggregation indicate that amyloid beta oligomerization and fibrillization pathways are independent and distinct. J Biol Chem. 2007; 282(14):10311–10324. [PubMed: 17284452]

Nussbaum JM, Schilling S, et al. Prion-like behaviour and tau-dependent cytotoxicity of pyroglutamylated amyloid-beta. Nature. 2012; 485(7400):651–655. [PubMed: 22660329]

Oddo S, Caccamo A, et al. Triple-transgenic model of Alzheimer's disease with plaques and tangles: intracellular Abeta and synaptic dysfunction. Neuron. 2003; 39(3):409–421. [PubMed: 12895417]

Oddo S, Caccamo A, et al. Temporal profile of amyloid-beta (Abeta) oligomerization in an in vivo model of Alzheimer disease. A link between Abeta and tau pathology. J Biol Chem. 2006; 281(3): 1599–1604. [PubMed: 16282321]

Perry G, Siedlak S, et al. Immunolocalization of the amyloid precursor protein within the senile plaque. Prog. Clin. Biol. Res. 1989; 317:1021–1025. [PubMed: 2513580]

Rasool S, Albay R 3rd, et al. Vaccination with a non-human random sequence amyloid oligomer mimic results in improved cognitive function and reduced plaque deposition and micro hemorrhage in Tg2576 mice. Mol Neurodegener. 2012; 7:37. [PubMed: 22866920]

Robakis NK. Mechanisms of AD neurodegeneration may be independent of Abeta and its derivatives. Neurobiol Aging. 2011; 32(3):372–379. [PubMed: 20594619]

Schmitz C, Rutten BP, et al. Hippocampal neuron loss exceeds amyloid plaque load in a transgenic mouse model of Alzheimer's disease. Am J Pathol. 2004; 164(4):1495–1502. [PubMed: 15039236]

Selkoe DJ, Podlisny MB, et al. Beta-amyloid precursor protein of Alzheimer disease occurs as 110- to 135-kilodalton membrane-associated proteins in neural and nonneural tissues. Proc. Natl. Acad. Sci. U. S. A. 1988; 85:7341–7345. [PubMed: 3140239]

Stern RA, Otvos L Jr. et al. Monoclonal antibodies to a synthetic peptide homologous with the first 28 amino acids of Alzheimer's disease beta-protein recognize amyloid and diverse glial and neuronal cell types in the central nervous system. Am. J. Pathol. 1989; 134:973–978. [PubMed: 2524164]

Szekely CA, Green RC, et al. No advantage of A beta 42-lowering NSAIDs for prevention of Alzheimer dementia in six pooled cohort studies. Neurology. 2008; 70(24):2291–2298. [PubMed: 18509093]

Terry RD. The pathogenesis of Alzheimer disease: an alternative to the amyloid hypothesis. J Neuropathol Exp Neurol. 1996; 55(10):1023–1025. [PubMed: 8857998]

Thal DR, Rub U, et al. Phases of A beta-deposition in the human brain and its relevance for the development of AD. Neurology. 2002; 58(12):1791–1800. [PubMed: 12084879]

Tomic JL, Pensalfini A, et al. Soluble fibrillar oligomer levels are elevated in Alzheimer's disease brain and correlate with cognitive dysfunction. Neurobiol Dis. 2009; 35(3):352–358. [PubMed: 19523517]

Wartha F, Henriques-Normark B. ETosis: a novel cell death pathway. Sci Signal. 2008; 1(21):pe25. [PubMed: 18506034]

Winton MJ, Lee EB, et al. Intraneuronal APP, not free Abeta peptides in 3xTg-AD mice: implications for tau versus Abeta-mediated Alzheimer neurodegeneration. J Neurosci. 2011; 31(21):7691–7699. [PubMed: 21613482]

Wirths O, Bayer TA. Intraneuronal Abeta accumulation and neurodegeneration: lessons from transgenic models. Life Sci. 2012; 91(23-24):1148–1152. [PubMed: 22401905]

Highlights

1. The amyloid specific antibody, M78, stains nuclei in 12 mo 3XTg-AD brain.

2. Neuritic plaques contain a core of nuclear M78 and diffuse chromatin.

3. M78 immunoreactive nuclei are significantly elevated in plaque stage A-B human brains.

4. Neuritic plaques arise from the death of neurons with intracellular amyloid.
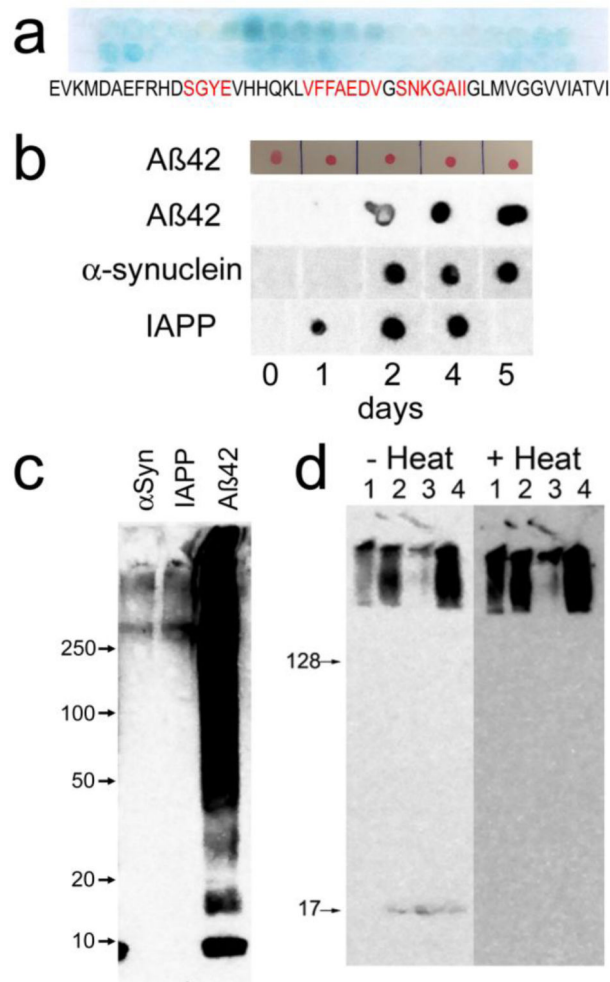
Fig. 1.
Characterization of M78 specificity. (a) Epitope mapping. M78 recognizes a discontinuous epitope in Aß consisting of 8-11, 18-24 and 26-32 (shown in red). (b) Kinetics of the appearance of M78 immunoreactivity during the aggregation of Aß42, α-synuclein and IAPP. Top strip: Aß42 samples stained with Ponceau S as a loading control. No immunoreactivity is detected immediately after dilution of monomer stock solutions in buffer. Bottom 3 strips: M78 immunoreactivity is observed for all 3 samples at a time of 1-2 days of incubation, which is coincident with fibril formation. (c) Western blotting of α-synuclein, IAPP and Aß42 samples after 3 days of incubation. M78 stains high molecular weight bands of α-synuclein, IAPP and Aß aggregates and a range of smaller sizes of Aß aggregates down to approximately the size of dimer. (d) Thermal denaturation of M78 epitope on western blots. After thermal denaturation, the 17 kDa tetrameric band disappears, while the staining of the high molecular weight material at the top of the gel increases slightly.
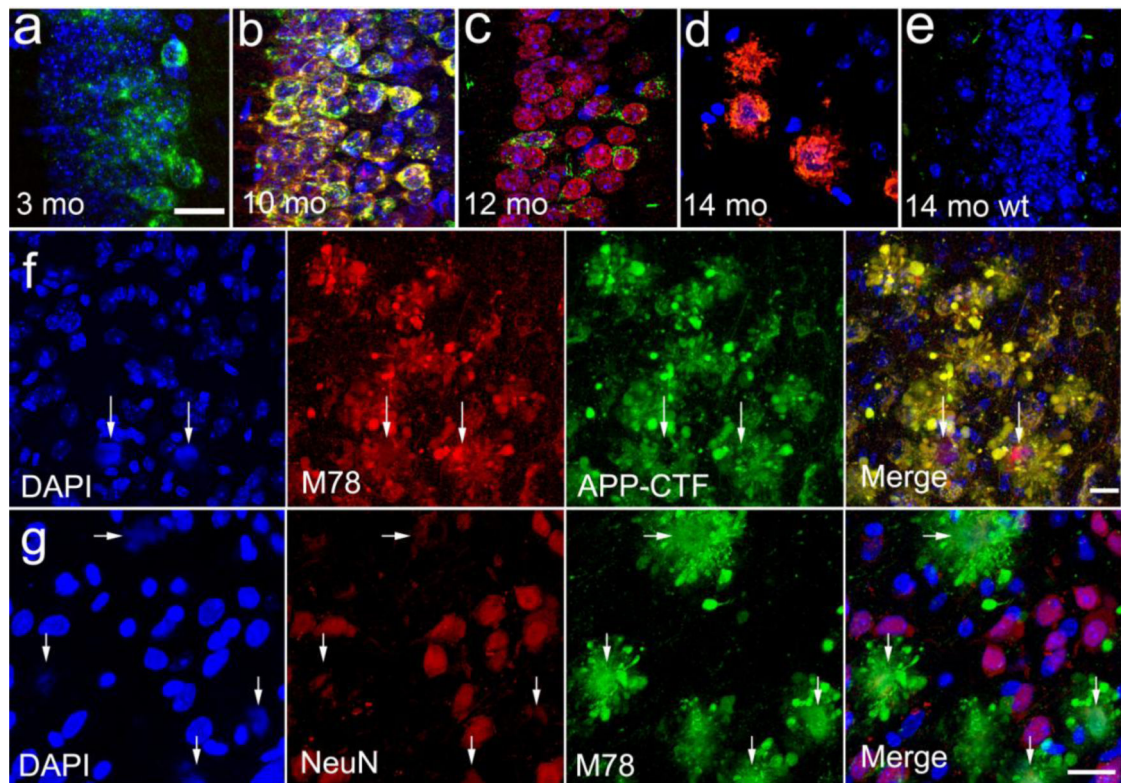
Fig. 2.
M78 labels intracellular amyloid and nuclei at intermediate times in 3XTg-AD mice. (a) At 3 mo, a subset of neurons exhibit elevated perinuclear 6E10 staining, but no M78 immunoreactivity is observed. (b) At 10 mo, M78 immunoreactivity (red) is primarily perinuclear and colocalized with 6E10 (green) in neurons. Nuclei are labeled with DAPI (blue). (c) At 12 mo, the M78 staining is primarily nuclear and is surrounded by 6E10 and M78 immunoreactivity in neurons. (d) At 14 mo, M78 staining is primarily restricted to plaques that stain weakly with 6E10. (e) No 6E10 or M78 staining is observed in 14 mo wild type brain. (a-c, e), CA1. (d), stratum oriens adjacent to CA1. (f). Triple label confocal immunofluorescence micrographs of 12 mo 3XTg-AD subiculum labeled with DAPI (blue), M78 (red) and anti-APPCTF antiserum (green). Arrows point to diffuse DAPI DNA staining that colocalizes with M78 immunoreactivity in the center of the neuritic plaques. The dystrophic neurites surrounding the plaque core are strongly positive for both M78 and APP-CTF. (g) The core of the M78+ neuritic plaques (green) also contains NeuN immunoreactivity (red) (arrows). The intensity of the DAPI image is enhanced compared to the merged image to show the details of the diffuse chromatin staining. Bar = 20 μm.
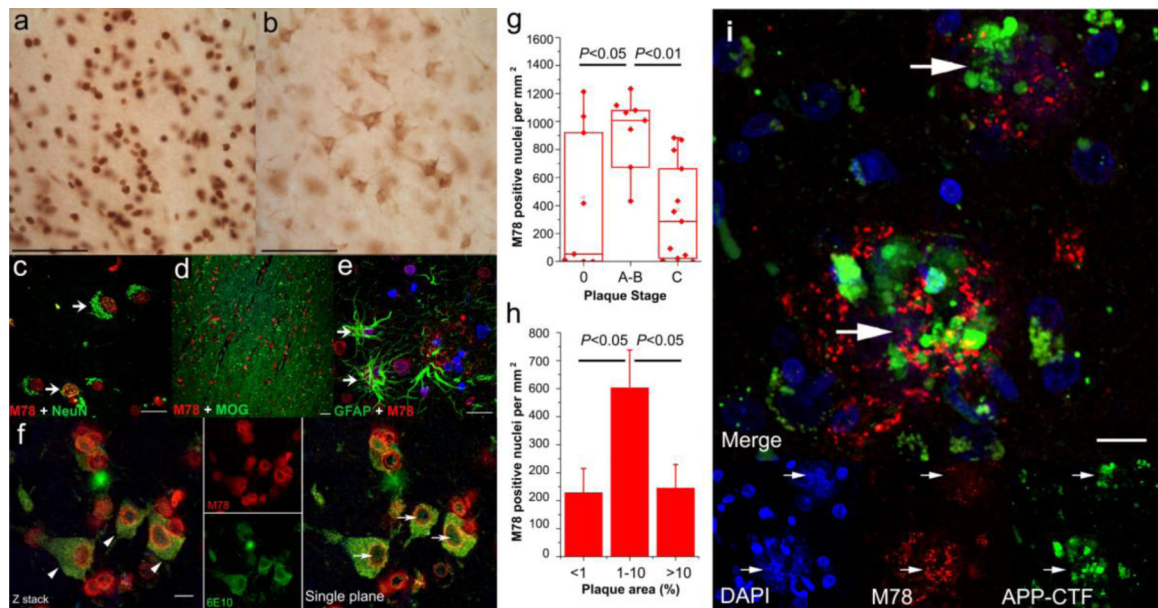
Fig. 3.
Intranuclear M78 immunoreactivity in human brain and correlation with plaque pathology. (a, b) Adjacent sections from the Broadman's B11 region were stained with M78 (a) or 6E10, (b). Bar = 100 μm. (c-e) Triple label immunofluorescence staining with M78 (red) and (c) NeuN (green), (d) myelin oligodendrocyte glycoprotein (green), or (e) glial fibrilliary acidic protein (GFAP), (green) and chromatin (DAPI, blue). Arrows point to co-localization of M78 and specific cell markers. Bar = 20 μm. (f), Double label immunofluorescence staining with M78 (red) and 6E10 (green). The arrows point to cells with neuronal morphology that stain for both M78 and 6E10. Bar = 20 μm. (g) M78 nuclear immunoreactivity correlates with intermediate stages of plaque area deposition (stage A and B) in the frontal cortex of subjects from the ADRC cohort. (h) Average counts per mm^2 of M78 positive nuclei in the frontal cortex of the combined ADRC and *The 90+ study* subjects are plotted against the OC positive plaque area fraction. The bars indicate the values of mean ± SEM. (i) Triple color immunofluorescence labeling of neuritic plaques with M78 (red), anti APP-CTF (green) and DAPI (blue). Arrows point to neuritic plaques containing a central core of diffuse DAPI fluorescence and M78 immunoreactivity with dystrophic neurites that stain for APP-CTF. The intensity of the DAPI image is enhanced compared to the merged image to show the details of the diffuse chromatin staining. Bar = 20 μm.
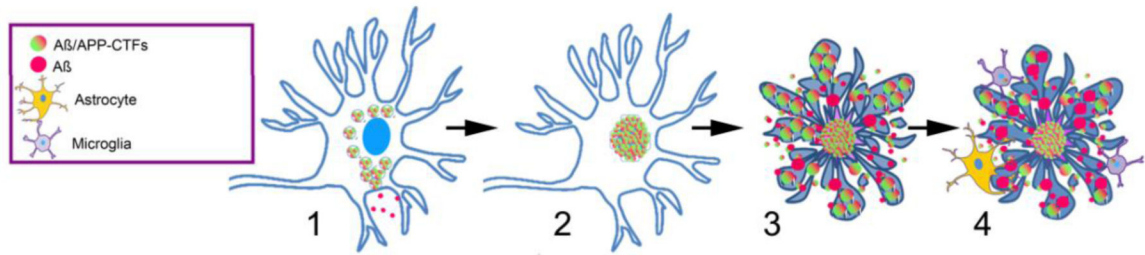
Fig.4.
Model for neuritic plaque development from neurons with accumulated intracellular and intranuclear amyloid. **Step 1**: An initial perturbation of intracellular APP metabolism within a single neuron leads to the early accumulation and aggregation of Aß, longer Aß containing fragments and APP-CTFs in a perinuclear localization. This perturbation may arise spontaneously due to an imbalance between the levels of secreted versus intracellularly retained Aß/APP or it could be initiated by the uptake of extracellular oligomeric Aß seeds by a prion-like mechanism. **Step 2**: misfolded Aß and APP CTFs accumulate in perinuclear lysosomal/autophagic vesicles without being degraded and within the nucleus. **Step 3**: the continuing build-up of perinuclear amyloid aggregates causes filling and distension of "dystrophic neurites" around the M78 positive nucleus. **Step 4**: Intracellular amyloid accumulation causes the demise and lysis of the neuron followed by infiltration of astrocytes and microglia that clear the cell debris and digest the protease sensitive parts of APP, leaving behind the protease resistant amyloid core.
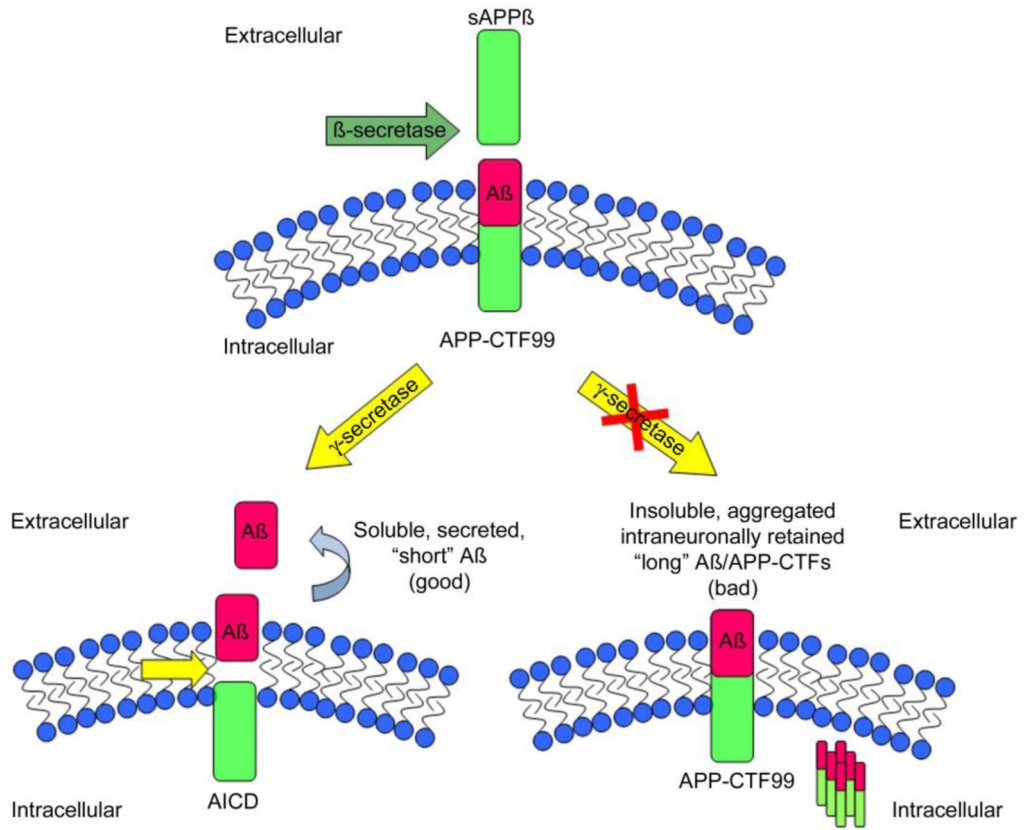
Fig.5.
Model for an "alternative" amyloid hypothesis.

BACE-mediated cleavage of APP results in the generation of soluble sAPPß and the transmembrane APP-CTF99. The next step in the amyloidogenic pathway consists of the γ-secretase-mediated cleavage of APP-CTF99. The high processivity of wild type γ-secretase releases soluble, short, "good" Aß species in the extracellular space and AICD in the cytosol. If the γ-secretase processivity is lost because of FAD-linked PS mutations or γ-secretase inhibition, the long Aß species and APP-CTF99 aggregate intracellularly and accumulate because of their intrinsic resistance to degradation, initiating the pathogenic mechanisms leading to cell death and formation of neuritic plaques.

Table 1

List of antibodies used in this study

Antibody	Type	Epitope / Immunogen	Source	Antigen retrieval	Working Dilution
M78	Rabbit mAb	Fibrillar Aβ 8-11, 18-24 and 26-32 of Aβ	Glabe lab	Not required (but stable IR under unmasking conditions listed below)	1-5 μg/ml
APP (C-term)	Rabbit pAb	751-770 of APP	Glabe lab	• Citrate and heat	1:200-1:500
OC	Rabbit pAb	Fibrillar Aβ	Glabe Lab	Not required	1-5 μg/ml
6E10	Mouse mAb	1-16 of Aβ	Covance, Princeton, New Jersey	•70% formic acid •Citrate and heat • 2N HCl in ddH$_2$O	1:500
4G8	Mouse mAb	18-22 of Aβ		• EDTA and heat	1:500
NeuN	Mouse mAb	Purified cell nuclei from mouse brain	Merk Millipore, Darmstadt, Germany	Citrate and heat	1:100
GFAP	Rabbit pAb	GFAP isolated from cow spinal cord	Dako, Glostrup, Denmark	None	1:1000
MOG (D-10)	Mouse mAb	176-247 of MOG of human origin	Santa Cruz Biotechnology, Dallas, Texas	None	1:100
MAP2	Chicken polyclonal	MAP2	Millipore	None	1:1000

Table 2

ADRC cohort

SUBJECT ID #	Age	Sex	PMI[a]	NPDx1[b]	Tangle Stage	Plaque Stage	MMSE[c]
11-02	91	F	4.82	Normal (MBC)	4	0	29
41-08	96	M	3.58	Normal (MBC)	2	0	29
15-02	88	F	5	Normal	2	0	29
09-06	112	F	3.5	Normal (MBC)	4	0	28
03-00	87	F	4.5	Normal	1	0	28
09-03	81	M	6.4	Normal (MBC)	2	0	27
35-08	94	M	3.87	Normal (MBC)	1	0	27
06-03	84.5	M	6.3	SDC	3	0	22
47-97	71	M	4.9	Normal	1	A	/
29-09	83	F	5.25	Normal (MBC)	4	A	30
07-03	84	F	4.25	Normal (MBC)	3	A	29
06-11	83	M	3.42	Normal (MVC)	5	C	24
12-03	81	F	7	SDC	5	C	23
03-03	79	M	3.5	AD	5	B	/
62-98	81	M	5	AD	5	B	12
09-01	82	F	6.6	AD	6	B	4
17-01	81	F	4.3	AD	5	B	0
34-99	77	F	5.4	AD/LBD	4	B	0
19-06	59	M	3.3	AD	6	C	/
05-09	57	F	3.17	AD	6	C	2
10-02	77.5	M	4.5	AD	4	C	19
10-11	90	F	6.58	AD	6	C	13
19-03	77	M	5	AD	6	C	11
25-10	57	F	3.17	AD	6	C	11
01-06	63	M	5.8	AD	6	C	10
14-03	76	M	3.75	AD	6	C	6
10-10	63	F	2.93	AD	6	C	2
04-02	83.2	M	3.5	AD	6	C	0

[a]PMI, post mortem index

[b]NPDx, neuropathological index; MBC, mild Braak changes; MVC, mild vascular changes; SDC, senile degenerative changes; AD, Alzheimer's disease; LBD, Lewy body dementia

[c]MMSE, mini mental state examination; n/a, not applicable

Table 3

90+ cohort

SUBJECT ID #	Age Range	Sex	PMI[a]	NPDx1[b]	Tangle Stage	Plaque Stage	MMSE[c]
19-09	95-99	M	5.50	Normal (MBC)	3	0	29
21-07	95-99	F	5.50	Normal (MBC)	2	0	29
23-09	100+	F	20.80	Normal (MBC)	2	0	25
27-06	90-94	M	6.80	Normal (MBC)	1	0	26
29-07	95-99	M	34.10	LBD	2	0	6
26-04	90-94	F	4.50	CBD	3	0	4
33-06	95-99	F	3.00	Normal (MBC)	2	0	4
23-07	95-99	F	7.70	Normal (MBC)	2	A	11
25-08	100+	F	4.00	Normal (MBC)	2	A	16
30-06	95-99	F	1.00	Normal (MBC)	3	A	26
37-06	95-99	M	3.50	Normal (MBC)	3	A	17
03-07	95-99	F	3.80	AD	5	B	29
06-06	100+	F	3.40	AD	5	B	17
24-07	95-99	M	14.50	AD	5	B	28
28-08	95-99	M	4.70	AD	5	B	18
37-05	100+	F	3.90	AD	5	B	29
02-08	95-99	F	5.10	AD	5	C	21
06-08	95-99	F	5.30	AD	6	C	0
27-07	95-99	F	4.10	AD	6	C	0
28-07	95-99	F	4.10	AD	6	C	25
37-08	95-99	F	5.40	AD	6	C	0

[a]PMI, post mortem index

[b]NPDx, neuropathological index; MBC, mild Braak changes; LBD, Lewy body dementia; CBD, corticobasal degeneration; AD, Alzheimer's disease;

[c]MMSE, mini mental state examination